Investigation of Dynamic Properties of a Novel Capacitive-Based Sensing Skin for Nondestructive Evaluation

Hussam Saleem[1], Austin Downey[1], Simon Laflamme[1,2], Matthias Kollosche[3], Filippo Ubertini[4]

[1] Dept. of Civil, Constr., and Env. Engineering, Iowa State University, Ames, IA, USA;
[2] Dept. of Electrical and Computer Engineering, Iowa State University, Ames, IA, USA;
[3] Institute of Physics and Astronomy, Potsdam University, Potsdam , Germany;
[4] Dept. of Civil and Environmental Engineering, University of Perugia, Perugia , Italy;

Abstract

A capacitive-based soft elastomeric strain sensor was recently developed by the authors for structural health monitoring applications. Arranged in a network configuration, the sensor becomes a sensing skin, where local deformations can be monitored over a global area. The sensor transduces a change in geometry into a measurable change in capacitance, which can be converted into strain using a previously developed electromechanical model. Prior studies have demonstrated limitations of this electromechanical models for dynamic excitations beyond 15 Hz, due to a loss in linearity in the sensor's response. In this paper, the dynamic behavior beyond 15 Hz is further studied, and a new version of the electromechanical model is proposed in order to accommodate dynamic strain measurements up to 40 Hz. This behavior is characterized by subjecting the sensor to a frequency sweep, and identifying possible sources of nonlinearities beyond 15 Hz. Results show possible frequency dependence of the materials' Poisson's ratio, which is successfully modeled and integrated into the electromechanical model. This demonstrates that the proposed sensor can be used for monitoring and evaluation of structural responses up to 40 Hz, a range covering the vast majority of the dominating frequency responses of civil infrastructures.

Keywords: nondestructive evaluation, structural health monitoring, soft elastomeric capacitor, capacitive sensor, vibration monitoring, sensing skin.

1 Introduction

Structural health monitoring (SHM) is defined as the automation of nondestructive evaluation (NDE), aimed at diagnosing, localizing, and prognosing structural damages in order to ensure public safety and structural integrity.[1] A particular challenge in SHM is associated with the magnitude of the geometries under assessment.[2] Existing sensing solutions are typically difficult to scale up to this mesoscale, because of technical and/or economic constraints. These include limitations in data interpretation, cost of installation, and scalability of the transducers.[3,4]

Recent advances in conductive polymers have enabled the development of scalable sensors. Their measurement principles are typically based on monitoring local states over global areas by deploying large arrays of flexible sensing substrates, analogous to sensing skins. For instance, Refs.[5–7] investigated carbon nanotube-based flexible strain sensors, and Refs.[8,9] proposed to utilize flexible sensing sheets of strain gauges.

The authors have recently proposed a highly scalable sensing skin for measurement of strain onto mesosurfaces.[10] The skin is composed of a dense network of soft elastomeric capacitors (SEC). The dielectric of an SEC is fabricated from a styrene-co-ethylene-co-butylene-co-styrene (SEBS) polymer matrix doped with titanium dioxide (TiO_2) nanoparticles, and the electrodes are constituted also from SEBS, but doped with carbon black (CB) particles. The SEC tranduces a change in its geometry into a measurable change in its capacitance. Other capacitive-based sensors have been proposed in literature for applications to humidity,[11] pressure,[12] strain,[13,14] and tri-axial measurements.[15] The proposed SEC differs from other sensors by being inexpensive and easy to fabricate, thus being highly scalable.

The utilization of the SEC technology for nondestructive evaluation has been demonstrated, including applications to fatigue crack detection,[16] surface strain measurements,[17] and extraction of deflection shapes.[18] These applications were focused on static and quasi-static behaviors. Recent investigations have been conducted on the characterization of the dynamic behavior of the SEC,[2] with applications to monitoring of vibration signatures.[19] Both studies concluded

that while the sensor can detect a change in dynamic properties, it only provides a linear response for mechanical excitations up to 15 Hz.

This paper investigates the dynamic response of the SEC for a wider range of excitation, considering mechanical frequencies up to 40 Hz, which covers a wide range of structural dynamics found in mesosystems. Note that unless noted otherwise, the term "frequency" in this paper refers to a mechanical frequency, not electrical. The electrical frequency-dependence of SEBS filled with titania has been thoroughly discussed in literature.[20,21] The objective of this paper is to develop an augmented electromechanical model that accommodates for possible sources of nonlinearity beyond 15 Hz, to enable SHM applications up to 40 Hz, a range covering the vast majority of the dominating frequency responses of civil infrastructures.

It is hypothesized that a possible source of nonlinearity arises from a non-negligible frequency-dependence of the SEBS's Poisson's ratio due to its viscoelasticity.[22–25] A laboratory-based study is conducted to test the hypothesis by investigating the change in the sensor's sensitivity as a function of frequency. Its dynamic behavior is characterized up to 40 Hz based on the assumption that this sensitivity is purely explained by the frequency-dependence of the Poisson's ratio. This model is used to develop an augmented electromechanical model for the SEC.

The rest of the paper is organized as follows. Section 2 presents the background on the technology, which includes the fabrication method and the original electromechanical model. Section 3 investigates the sensor's dynamic behavior, and develops an augmented electromechanical model that covers excitations up to 40 Hz. Section 4 concludes the paper.

2 Background

This section provides a background on the SEC technology. It includes a description of the fabrication process and a derivation of the original electromechanical model.

2.1 Fabrication Method

The fabrication process of an SEC is described in details in Ref.[16] Briefly, SEBS is dissolved in toluene, and the solution is mixed with 15 vol% TiO_2 to increase permittivity and durability of the polymer. Uniform dispersion of the nanoparticles is obtained via sonication using a sonic dismembrator for 10 min. The sonicated solution is then casted on a 80 mm $\times$ 80 mm non-stick glass plate and left overnight for the solvent to evaporate, which creates the dielectric. In the meanwhile, 10 vol% CB is added to another SEBS-toluene solution and dispersed in a sonic bath for 6 hours. The resulting conductive paint is applied onto the top and bottom surfaces of the dielectric to create electrodes. Copper tape is embedded in the wet conductive paint, on each sides of the dielectric, to enable mechanical connections to the data acquisition system (DAQ). Figure 1(a) is a picture of the resulting SEC.

2.2 Electromechanical Model

The SEC is designed to measure in-plane strain along the $x-y$ plane shown in Fig. 1(b). Assuming low electrical frequency measurements (<1 kHz), the SEC can be simplified as a non-lossy parallel plate capacitor with capacitance C

$$C = e_0 e_r \frac{A}{h} \tag{1}$$

where $e_0 = 8.854$ pF/m is the vacuum permittivity, e_r is the polymer relative permittivity, $A = w \cdot l$ is the area of the sensor electrodes of width w and length l, and h is the thickness of the dielectric. Assuming small strain, one can take the differential of Eq. (1) to obtain an expression for the change in capacitance ΔC:

$$\frac{\Delta C}{C} = \left(\frac{\Delta l}{l} + \frac{\Delta w}{w} - \frac{\Delta h}{h} \right) = \varepsilon_x + \varepsilon_y - \varepsilon_z \tag{2}$$

where ε_x, ε_y and ε_z are strains in the x, y and z directions as shown in Fig. 1(b). An expression relating ε_z to ε_x and ε_y can be obtained using Hooke's law for plane stress conditions:

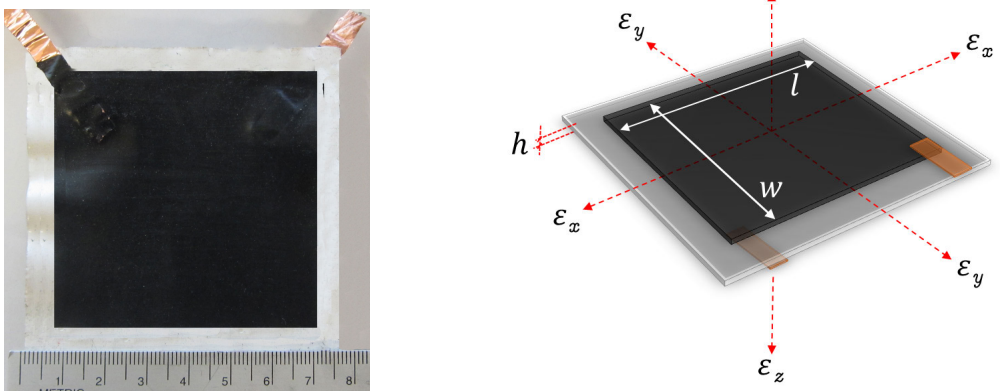

(a) (b)

Figure 1: soft elastomeric capacitor (SEC): (a) picture (75 x 75 mm^2); and (b) reference axis

$$\varepsilon_z = -\frac{\nu}{1-\nu}(\varepsilon_x + \varepsilon_y) \tag{3}$$

The final form of the electromechanical model is obtained by integrating Eq. (3) in Eq. (2)

$$\frac{\Delta C}{C} = \lambda(\varepsilon_x + \varepsilon_y) \tag{4}$$

where

$$\lambda = \frac{1}{1-\nu} \tag{5}$$

is the gauge factor. For SEBS, $\nu \approx 0.49$,[26] which yields a gauge factor $\lambda \approx 2$.

3 Investigation of Dynamic Behavior

In this section, the behavior of the SEC is investigated in the frequency range 1-40 Hz. Response linearity and sensitivity as a function of a frequency-dependent Poisson's ratio are studied. Finally, an augmented electromechanical model where ν is allowed to be frequency-dependent in Eq. (12) is presented.

3.1 Methodology

The test setup is shown in Fig. 2(a). It consists of an aluminum plate of dimensions 432 x 102 x 0.68 mm^3 excited axially, onto which an SEC is adhered. Two resistive strain gauges (RSGs) are installed onto the back of the plate opposite to the SEC, measuring strain in both the x and y directions independently, where x denotes the direction of the applied load and y is transverse to the load and in-plane with the SEC. Data from the SEC are recorded using an off-the-shelf DAQ (ACAM PCAP-02) at a sampling rate of 250 Hz.

The axial excitation is provided by a servo-hydraulic testing machine, and consists of a time-varying harmonic tensile force sweeping from 1 to 40 Hz in 1 Hz increments. The strain time history is shown in Figure 2(b). Due to equipment limitations, the displacement decreased with increasing frequency as it is observed in Figure 2(b).

Parameters of interest in the study of the dynamic behavior of the SEC are the linearity of the response and the gauge factor as a function of the excitation frequency. For each frequency of interest, the time histories of both the load input and the sensor's capacitance output were extracted using a window function. A band-pass filter designed

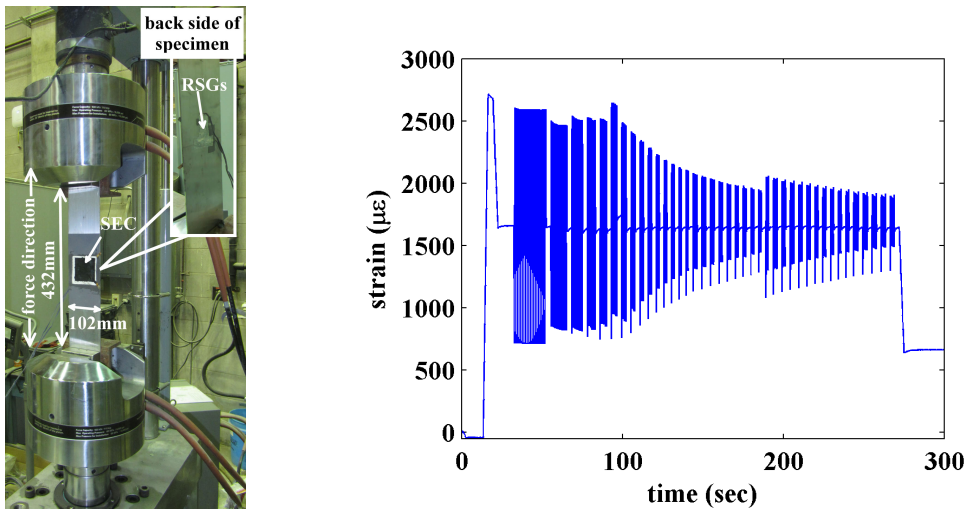

(a) (b)

Figure 2: (a) test setup and (b) RSG strain data

around this frequency was applied to both time series (input and output) to reduce noise. The linearity was assessed by plotting the filtered output versus the filtered input, and the experimental gauge factor was back-calculated from Eq. (11) using the measured ε_x and ε_y from the resistive strain gauges and ΔC.

Figure 3 shows the filtered time series following this methodology at three particular frequencies: 1, 20 and 40 Hz, which represent the lowest, middle and highest frequencies in the sweep. A salient feature in the plots is the increase in the level of noise with the increase in frequency. This can be attributed to electromagnetic interference (EMI), despite careful attention to minimize such noise in the experimental setup (e.g., by utilizing shielded cables and grounding of components).

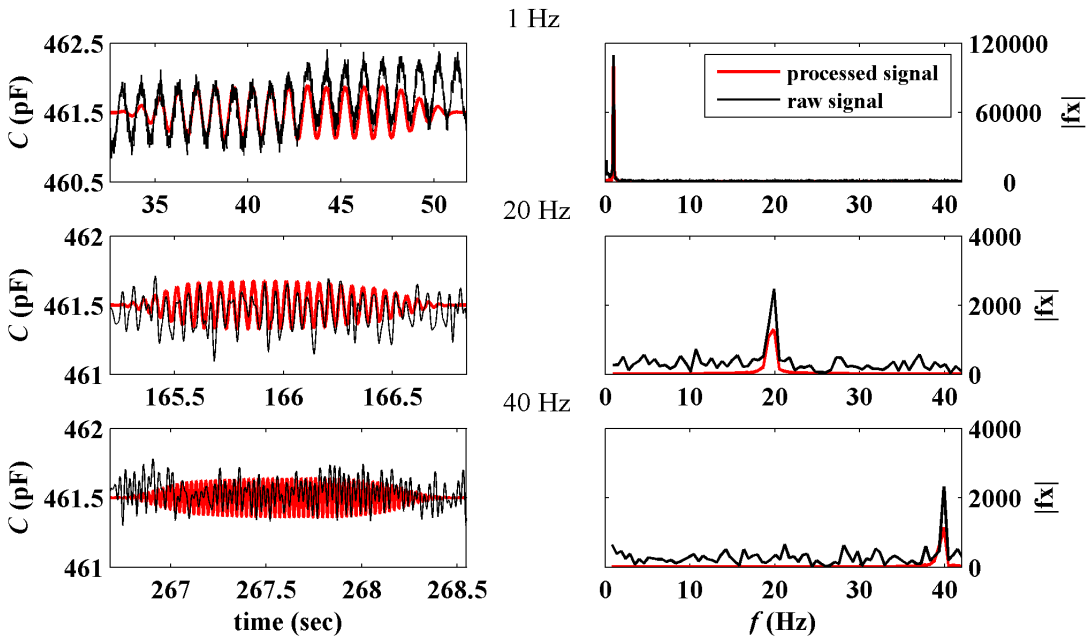

Figure 3: Time histories and Fourier transforms of signals provided by RSGs and SEC in the harmonic tensile load test

Figure 4 shows the wavelet transform of the raw signal (Figure 4(a)) compared against the processed signal (Figure 4(b)), using morlet wavelets. The wavelet transform is normalized at each discrete time interval to the highest wavelet amplitude. The black line is the input frequency content. Results validate the signal processing methodology, and show good agreement between the dynamic input and sensor output across the entire frequency range from 1 to 40 Hz.

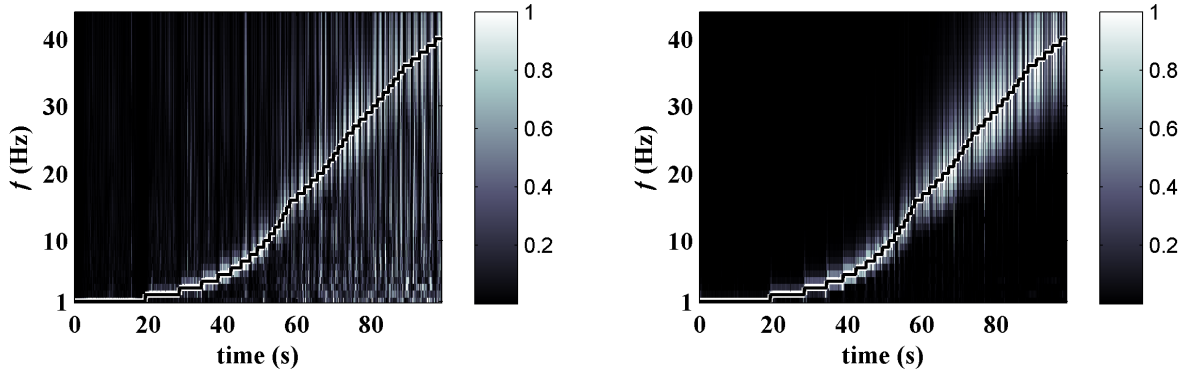

(a) (b)

Figure 4: wavelet transform of the a) raw and the b) processed data

3.2 Results

The sensor linearity and sensitivity are studied through the investigation of the sensor's response as a function of frequencies. Figure 5 are plots of the response of the SEC against the measured additive strain $\varepsilon_x + \varepsilon_y$. The red line is the linear fit obtained via linear regression. The quality of the linear fit represents the linearity of the sensor, while the slope of the regression represents its sensitivity $S = \Delta C/(\varepsilon_x + \varepsilon_y)$. The root means square error (RMSE) is used as a performance measure for linearity, plotted in Fig. 6. The figure shows higher error at lower frequency excitations. This could be attributed to the higher magnitude of the strain input at lower frequencies. Yet, the overall RMSE shows a good linearity of the sensor.

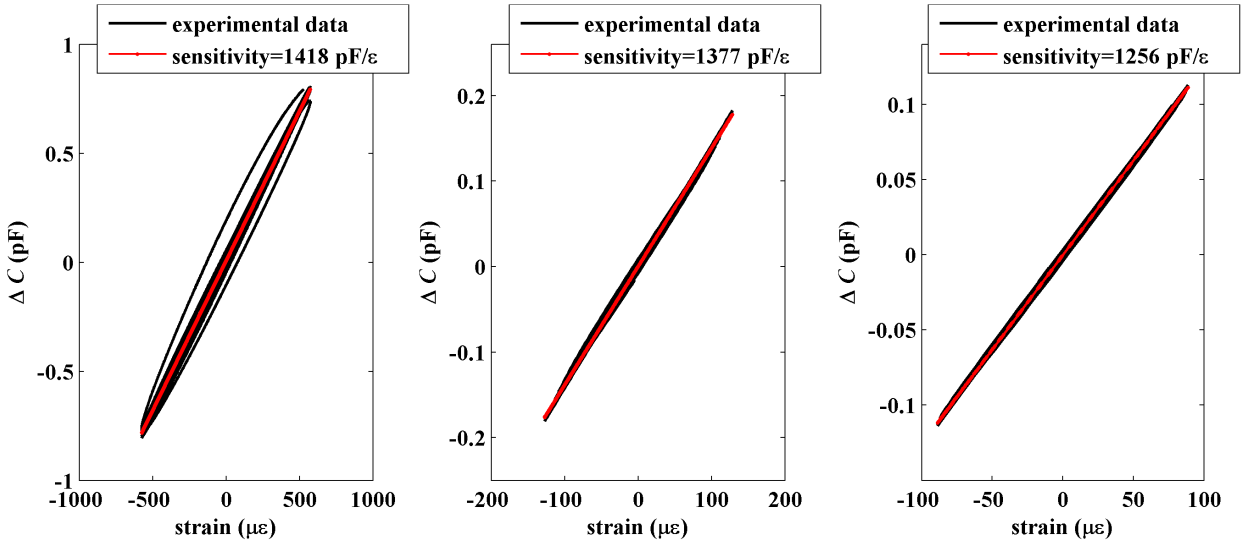

(a) (b) (c)

Figure 5: sensitivity and linearity of the sensor signal at: (a) 1 Hz; (b) 20 Hz; and (c) 40 Hz

Results from Fig. 5 show a decrease in sensitivity with increasing frequency. This can also be observed in the plotted gauge factor, calculated from the experimental results, shown in Figure 7. A two-term power series provided the best fit of the experimental gauge factor data. This fit illustrates the apparent reduction in the gauge factor as the frequency increases. The sensitivity S is reduced by 2.9% at 20 Hz and 11.5% at 40 Hz with respect to the reference S at 1 Hz as shown in Figures 5a, 5b, and 5c respectively.

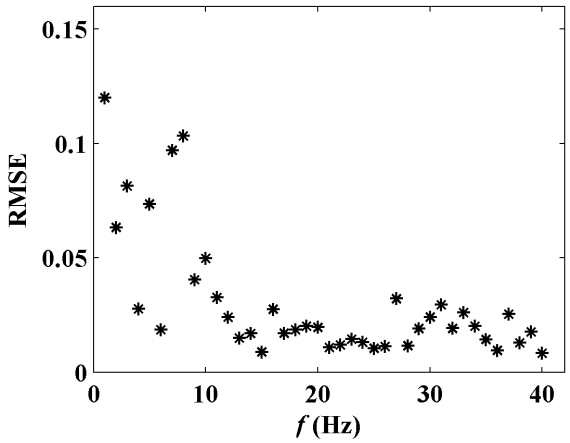

Figure 6: root mean square fitting error for the capacitance data

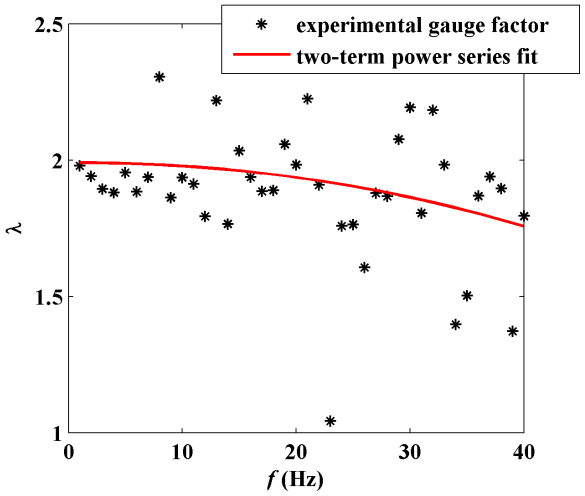

Figure 7: experimental gauge factor

As explained in the introduction, we model the change in the sensor's sensitivity assuming that it can be explained by the complex Poisson's ratio of the material. Consider the strain modeled as a complex component:[23]

$$\begin{aligned} \varepsilon_x(t) &= \hat{\varepsilon}_x e^{j\omega t} \\ \varepsilon_y(t) &= \hat{\varepsilon}_y e^{j\omega(t-\Delta t)} = \hat{\varepsilon}_y e^{j(\omega t - \delta_\nu)} \end{aligned} \tag{6}$$

where t is the time, $\hat{\varepsilon}_x$ is the amplitude of the axial strain, $\hat{\varepsilon}_y$ is the amplitude of the lateral strain modeled with the same frequency response as $\hat{\varepsilon}_x$, but with a phase lag $\delta_\nu = \omega\Delta t$. The complex Poisson's ratio is the ratio of the lateral to the axial strains:

$$\bar{\nu}(j\omega) = \frac{\varepsilon_y(t)}{\varepsilon_x(t)} = \frac{\hat{\varepsilon}_y}{\hat{\varepsilon}_x} e^{-j\delta_\nu} = \frac{\hat{\varepsilon}_y}{\hat{\varepsilon}_x}(\cos\delta_\nu - j\sin\delta_\nu) = \nu_d(\omega) - j\nu_l(\omega) = \nu_d(\omega)[1 - j\eta_\nu(\omega)] \tag{7}$$

where ν_d is the dynamic Poisson's ratio, ν_l is the loss component, and η_ν is the Poisson's loss factor:

$$\eta_\nu(\omega) = \frac{\nu_l(\omega)}{\nu_d(\omega)} \tag{8}$$

The absolute value of $\bar{\nu}(j\omega)$ (Eqn. 7) provides an expression that relates ν_d and η_ν to the magnitude of the Poisson's ratio $|\bar{\nu}(j\omega)|$:

$$|\bar{\nu}(j\omega)| = \frac{\hat{\varepsilon}_y}{\hat{\varepsilon}_x} = (\nu_d^2 + \nu_l^2)^{1/2} = \nu_d(1 + \eta_\nu^2)^{1/2} \tag{9}$$

Further, it is shown in Ref.[23] that, assuming an incompressible material ($\nu_d \approx 0.5$), the Poisson's lost factor relates to the materials' shear loss modulus η_G through the following expression:

$$\frac{\eta_\nu(\omega)}{\eta_G(\omega)} \approx 1 - 2\nu_d(\omega) \tag{10}$$

We obtained a set of experimental values for η_G by conducting a dynamic mechanical analysis (DMA) of the studied material. Fig. 8 presents the results. Measurements indicate an increase in the real part of the shear modulus G' and the shear loss modulus $\eta_G = G^{\text{“}}/G$ with increasing frequency. This phenomenon can be attributed to the polymer-particles and particle-particle interactions.[27]

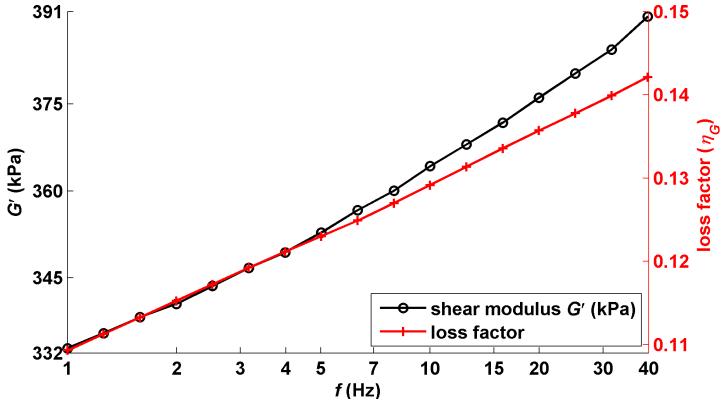

Figure 8: Storage moduli (G') and loss factor (η_G) as functions of frequency for the SEC composite (SEBS+TiO_2).

Values for η_G obtained from the DMA, combined with the experimental Poisson's ratio coefficients derived from S and Eqn. 12, can be used with Eqns. 9 and 10 to find ν_d and η_ν. Figures. 9a and 9b show the results obtained over the frequency range 1-40 Hz. Results show a decreasing dynamic Poisson's ratio ν_d and an increasing Poisson's loss factor η_ν with increasing frequency. The red solid line is the data fit using a two-term power series fit. This fit can be used to characterize the changes in ν_d and η_ν as a function of ω, and yield mathematical expressions to generate the adjusted electromechanical model.

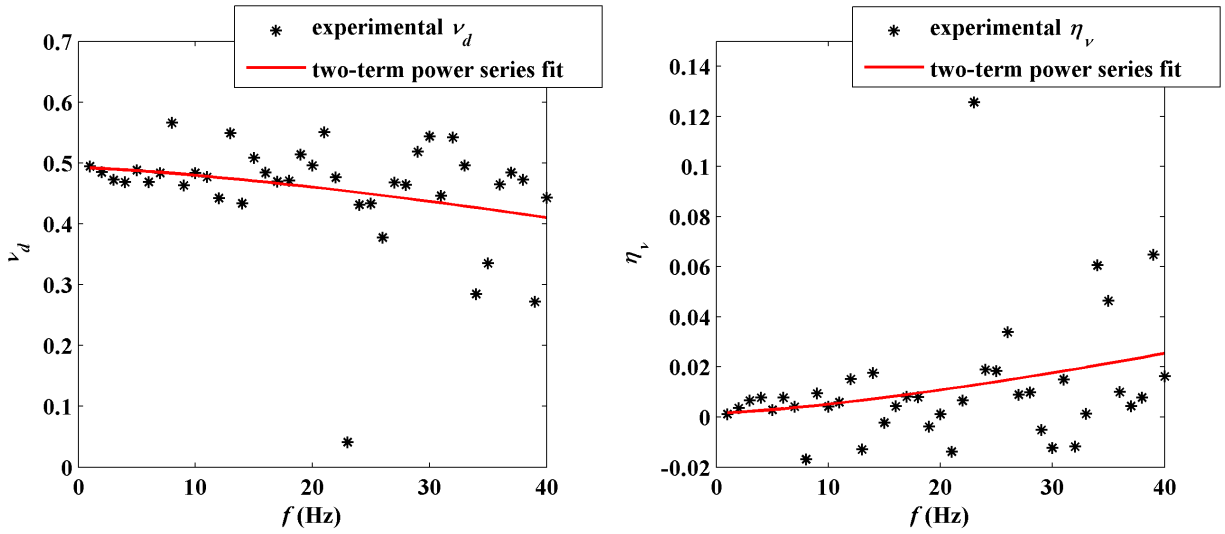

(a) (b)

Figure 9: a) Dynamic Poisson's ratio and b) Poisson's ratio loss factor plotted against frequency

3.3 Adjusted Electromechanical Model

Using results from the previous section, we can generate an adjusted electromechanical model that accounts for the change in the material's behavior as the frequency increases. The proposed model is a variation of Eqn. 11:

$$\frac{\Delta C}{C} = \lambda_{\text{adj}}(\varepsilon_x + \varepsilon_y) \tag{11}$$

where

$$\lambda_{\text{adj}} = \frac{1}{1 - \nu_{\text{adj}}} \tag{12}$$

and

$$\nu_{\text{adj}}(\omega) = \nu_d(\omega)(1 + \eta_\nu^2(\omega))^{1/2} \tag{13}$$

where the expressions for ν_d and η_ν are directly obtained from the investigation in the previous section:

$$\begin{aligned} \nu_d(\omega) &= -4.65 \times 10^{-5}\omega^{1.35} + 0.49 \\ \eta_\nu(\omega) &= 1.27 \times 10^{-5}\omega^{1.36} + 0.0016 \end{aligned} \tag{14}$$

where the adjusted electromechanical model is valid up to 40 Hz.

Figure 10 shows the RMSE on the estimation of λ as a function of frequency, for both the original and adjusted models. Table I summarizes the results for frequency ranges of interest. Results show that the adjusted model provides an overall improvement on the estimation of RMSE_λ by 14.3% over the range 1-40 Hz. The vast majority of this improvement is from the estimation in the 16-40 Hz range, where the adjusted model improves the estimation on RMSE_λ by 15.8%. This demonstrates the superiority of the new model over the original model. Note that the RMSE_λ over the range 1-15 Hz is only marginally improved, which demonstrates the validity of the original model over the 1-15 Hz range.

Table I: Average RMSE_λ

	range		
	1-40 Hz	1-15 Hz	16-40 Hz
original model	0.266	0.146	0.317
adjusted model	0.228	0.143	0.267
improvement	14.3%	2.05%	15.8%

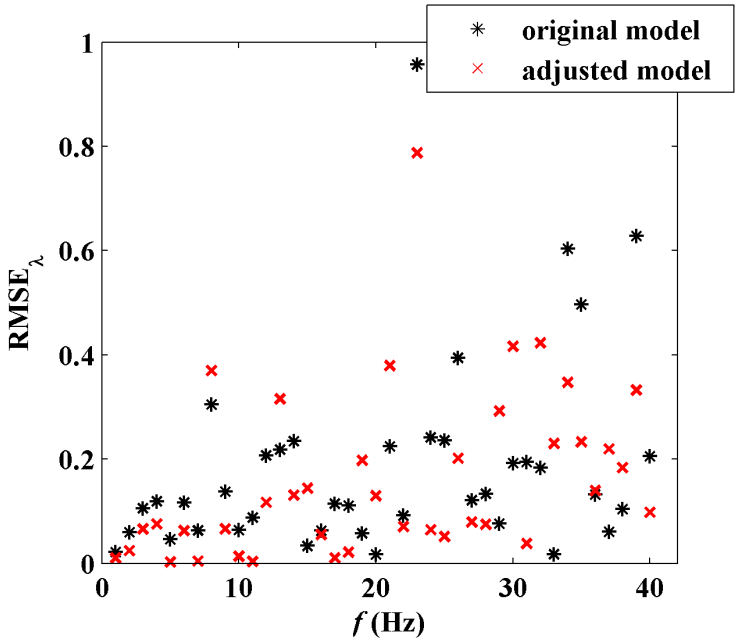

Figure 10

4 Conclusion

In this paper, we have presented a novel sensor for nondestructive evaluation. The sensor is a soft elastomeric capacitor (SEC). Arranged in a network configuration, it is analogous to sensing skin, in the sense that it can measure discrete changes over a global area. Previous work on the SEC developed an electromechanical model, which showed to be valid for excitations up to 15 Hz. Here, we proposed to adjust the electromechanical model to cover a broader range of excitations, up to 40 Hz.

We hypothesized that a possible source of nonlinearities arose from a non-negligible frequency-dependence of the SEBS's Poisson's ratio due to its viscoelasticity. An empirical study on the SEC's material response as a function of frequency was conducted. Results show that the experimental Poisson's ratio decreased with increasing mechanical frequency. This relationship was successfully modeled as a complex Poisson's ratio, and led to an adjusted electromechanical model that could account for the sensor's nonlinearities up to 40 Hz. Note that while it is possible that the nonlinearities come from other sources, this model can still be used to transduce changes in capacitance into strain.

By covering an excitation range up to 40 Hz, the adjusted electromechanical model enables measurements over a frequency range that covers the vast majority of dynamic responses in civil structures. It empowers the SEC technologies with dynamic measurement capabilities, useful for vibration-based structural health monitoring and nondestructive evaluation.

Acknowledgements

The work presented in this paper is partially funded by a fellowship award from the American Society for Nondestructive Testing. The development of the SEC technology is supported by grant No. 1001062565 from the Iowa Alliance for Wind Innovation and Novel Development and grant No. 13-02 from the Iowa Energy Center. This work is also partially funded under the U.S. National Science Foundation Grant No. 4782025 which supports the activities of the Integrative Graduate Education and Research Traineeship (IGERT) in Wind Energy Science, Engineering and Policy (WESEP) at Iowa State University.

REFERENCES

[1] T. Harms, S. Sedigh, F. Bastianini, Structural Health Monitoring of Bridges Using Wireless Sensor Networks, Instrumentation & Measurement Magazine, IEEE 13 (6) (2010) 14–18.

[2] S. Laflamme, F. Ubertini, H. Saleem, A. DAlessandro, A. Downey, H. Ceylan, A. L. Materazzi, Dynamic characterization of a soft elastomeric capacitor for structural health monitoring, Journal of Structural Engineering.

[3] C. R. Farrar, N. A. Lieven, Damage prognosis: the future of structural health monitoring, Philosophical Transactions of the Royal Society A: Mathematical, Physical and Engineering Sciences 365 (2007) 879–885.

[4] S. Laflamme, M. Kollosche, J. J. Connor, G. Kofod, Robust flexible capacitive surface sensor for structural health monitoring applications, Journal of Engineering Mechanics.

[5] I. Kang, M. J. Schulz, J. H. Kim, V. Shanov, D. Shi, A carbon nanotube strain sensor for structural health monitoring, Smart materials and structures 15 (3) (2006) 737.

[6] K. J. Loh, T.-C. Hou, J. P. Lynch, N. A. Kotov, Carbon nanotube sensing skins for spatial strain and impact damage identification, Journal of Nondestructive Evaluation 28 (1) (2009) 9–25.

[7] R. K. Srivastava, V. S. M. Vemuru, Y. Zeng, R. Vajtai, S. Nagarajaiah, P. M. Ajayan, A. Srivastava, The strain sensing and thermal–mechanical behavior of flexible multi-walled carbon nanotube/polystyrene composite films, Carbon 49 (12) (2011) 3928–3936.

[8] S. Tung, Y. Yao, B. Glisic, Sensing sheet: the sensitivity of thin-film full-bridge strain sensors for crack detection and characterization, Measurement Science and Technology 25 (7) (2014) 075602.

[9] Y. Hu, W. S. Rieutort-Louis, J. Sanz-Robinson, L. Huang, B. Glisic, J. C. Sturm, S. Wagner, N. Verma, Large-scale sensing system combining large-area electronics and cmos ics for structural-health monitoring, Solid-State Circuits, IEEE Journal of 49 (2) (2014) 513–523.

[10] S. Laflamme, M. Kollosche, J. J. Connor, G. Kofod, Robust flexible capacitive surface sensor for structural health monitoring applications, Journal of Engineering Mechanics 139 (7) (2012) 879–885.

[11] H. P. Hong, K. H. Jung, N. K. Min, Y. H. Rhee, C. W. Park, A highly fast capacitive-type humidity sensor using percolating carbon nanotube films as a porous electrode material, in: Sensors, 2012 IEEE, 2012, pp. 1–4.

[12] D. J. Lipomi, M. Vosgueritchian, B. C. K. Tee, S. L. Hellstrom, J. A. Lee, C. H. Fox, Z. Bao, Skin-like pressure and strain sensors based on transparent elastic films of carbon nanotubes, Nature Nanotechnology 6 (12) (2011) 788–792.

[13] K. Arshak, D. McDonagh, M. Durcan, Development of new capacitive strain sensors based on thick film polymer and cermet technologies, Sensors and Actuators A: Physical 79 (2) (2000) 102 – 114.

[14] M. Suster, J. Guo, N. Chaimanonart, W. Ko, D. Young, A high-performance mems capacitive strain sensing system, Microelectromechanical Systems, Journal of 15 (5) (2006) 1069–1077.

[15] J. A. Dobrzynska, M. A. M. Gijs, Polymer-based flexible capacitive sensor for three-axial force measurements, Journal of Micromechanics and Microengineering 23 (1) (2013) 015009.

[16] S. Kharroub, S. Laflamme, C. Song, D. Qiao, B. Phares, J. Li, Smart sensing skin for detection and localization of fatigue cracks, Smart Materials and Structures 24 (6) (2015) 065004.

[17] J. Wu, C. Song, H. S. Saleem, A. Downey, S. Laflamme, Network of flexible capacitive strain gauges for the reconstruction of surface strain, Measurement Science and Technology 26 (5) (2015) 055103.

[18] S. Laflamme, H. Saleem, B. Vasan, R. Geiger, D. Chen, M. Kessler, K. Rajan, Soft elastomeric capacitor network for strain sensing over large surfaces, Mechatronics, IEEE/ASME Transactions on 18 (6) (2013) 1647–1654.

[19] F. Ubertini, S. Laflamme, H. Ceylan, A. L. Materazzi, G. Cerni, H. Saleem, A. DAlessandro, A. Corradini, Novel nanocomposite technologies for dynamic monitoring of structures: a comparison between cement-based embeddable and soft elastomeric surface sensors, Smart Materials and Structures 23 (4) (2014) 045023.

[20] H. Stoyanov, M. Kollosche, D. N. McCarthy, G. Kofod, Molecular composites with enhanced energy density for electroactive polymers, Journal of Material Chemistry 20 (2010) 7558–7564.

[21] M. Kollosche, H. Stoyanov, S. Laflamme, G. Kofod, Strongly enhanced sensitivity in elastic capacitive strain sensors, Journal of Materials Chemistry 21 (23) (2011) 8292–8294.

[22] N. Tschoegl, W. Knauss, I. Emri, Poisson's ratio in linear viscoelasticity a critical review, Mechanics of Time-Dependent Materials 6 (1) (2002) 3–51.

[23] T. Pritz, The poisson's loss factor of solid viscoelastic materials, Journal of Sound and Vibration 306 (35) (2007) 790 – 802.

[24] H. P. Kugler, R. G. Stacer, C. Steimle, Direct measurement of poisson's ratio in elastomers, Rubber Chemistry and Technology 63 (4) (1990) 473–487.

[25] Y. Wada, R. Ito, H. Ochiai, Comparison between mechanical relaxations associated with volume and shear deformations in styrene-butadiene rubber, Journal of the Physical Society of Japan 17 (1) (1962) 213–218.

[26] A. Wilkinson, M. Clemens, V. Harding, The effects of sebs-g-maleic anhydride reaction on the morphology and properties of polypropylene/pa6/sebs ternary blends, Polymer 45 (15) (2004) 5239 – 5249.

[27] The effect of fillerfiller and fillerelastomer interaction on rubber reinforcement, Composites Part A: Applied Science and Manufacturing 36 (4) (2005) 449 – 460.